An Experimental Demonstration of an Energy Efficient DMT Technique for LiFi Systems

An Experimental Demonstration of an Energy Efficient DMT Technique for LiFi Systems

Mohamed Sufyan Islim and Harald Haas

School of Engineering, Institute for Digital Communications, LiFi R&D Centre, the University of Edinburgh, King's Buildings, Mayfield Road, Edinburgh, EH9 3JL, UK
Email: {m.islim, h.haas}@ed.ac.uk

***Abstract*—A direct current (DC) bias is required in DC-biased optical orthogonal frequency division multiplexing (DCO-OFDM) to enable visible light communication (VLC). However, the addition of the DC-bias leads to electrical and optical power inefficiency. An experimental demonstration of an energy efficient superposition modulation technique is presented based on augmented spectral efficiency discrete multitone (ASE-DMT) transmission. Significant energy savings of up to 14.27 dB are achieved in comparison with DCO-OFDM at low DC bias. The results highlight the potential of ASE-DMT in spectrum and energy efficient light fidelity (LiFi) systems.**

I. Introduction

The limited availability of radio frequency (RF) spectrum is becoming an ever more important challenge as the demand for wireless broadband access increases [1]. Visible light communication (VLC) offers a low-cost solution to the looming spectrum crunch due to the availability of inexpensive front-end devices. The ubiquitous availability of light sources enables the opportunity of creating a dense network of access points. VLC is also a unique option in scenarios where the RF propagation is considered to be hazardous, such as hospital theaters and petrochemical plants. Data rates in the excess of 100 Gb/s are predicted to be achievable when the complete visible spectrum is utilized [2]. Light fidelity (LiFi) is the high speed bidirectional light-based networking solution that is proposed to work seamlessly with other RF access technologies [3], [4]. LiFi can support multiuser access and handover between light-based access points.

Incoherent optical sources are widely used in LiFi transmitters due to their low cost and simple system design. The adoption of these transmitters limit the signaling to intensity modulation and direct detection (IM/DD). Orthogonal frequency division multiplexing (OFDM) is a proven candidate for both wired and wireless IM/DD-based systems due to its resilience to the frequency selective fading [3]. However, the power penalty of direct current (DC) biased optical OFDM (DCO-OFDM) increases at high spectral efficiency values due to the DC bias requirements [5]. Pulse-amplitude modulation discrete multitone modulation (PAM-DMT) is introduced to provide an energy efficient optical OFDM alternative to DCO-OFDM [6]. However, its energy efficiency degrades at high modulation orders due to the restrictions imposed on the frame structures [7]. PAM-DMT uses pulse-amplitude modulation (PAM) on the imaginary part of the subcarriers. Therefore, the bit error ratio (BER) performance of M_{PAM} is equivalent to the performance of M_{DCO}^2-quadrature amplitude modulation (QAM). The BER performance gain of PAM-DMT degrades as the constellation size of M_{PAM} increases in comparison with DCO-OFDM at the same spectral efficiency.

The energy efficiency is a desired feature in communication systems. It is essentially required at the mobile user-end to reduce the power consumption. Dimming is recently becoming an indispensable feature for general lighting systems. Moreover, the dimming support of the cabin illumination system is a compulsory feature for airplanes. Low DC bias is required to enable the dimming of the light source. DCO-OFDM is not the best suited to support dimming due to the required DC bias. A novel computational and energy efficient superposition modulation technique is proposed in our previous work [7]. The selective loading algorithm in augmented spectral efficiency discrete multitone (ASE-DMT) allows multiple streams of PAM-DMT to be superimposed without affecting the demodulation of each individual stream. ASE-DMT avoids spectral efficiency losses of PAM-DMT and provides energy efficiency gains over DCO-OFDM and PAM-DMT. A successful demonstration of 4-PAM ASE-DMT using a novel single inverse fast Fourier transform (IFFT) transmitter was achieved recently at a data rate of 18.4 Gb/s over a 10 km single mode fiber [8].

An experimental study on the performance of ASE-DMT is presented in this paper at unprecedented high spectral efficiency values up to 32-PAM. The performance of ASE-DMT is compared with DCO-OFDM and PAM-DMT using a blue light emitting diode (LED) (Vishay VLMB1500) and an infra-red (IR) vertical-cavity surface-emitting laser (VCSEL) (OPV300). Blue LEDs are widely used in light sources for general illumination purposes. Therefore, the choice of the blue LED is particularly interesting to demonstrate the performance of ASE-DMT for the dimming applications in VLC. Whereas, the IR VCSEL is suitable for the up-link of LiFi systems.

The implementation of DCO-OFDM in this paper is similar to the demonstration presented in [9], while the implementations of PAM-DMT and ASE-DMT are presented in Section II. The experimental setup is detailed in Section III. The results are discussed in Section IV and the conclusions are summarized in Section V.

II. An Implementation of ASE-DMT

The waveform in ASE-DMT is generated by the selective loading of imaginary and real components of the sub-

carriers using MATLAB®. A pseudo-random series of bits is encoded into PAM symbols. The ASE-DMT stream at the first modulation depth $d = 1$ is exactly equivalent to a PAM-DMT stream [6]. Therefore, the implementation of ASE-DMT with one modulation depth $D = 1$ is identical to a PAM-DMT implementation. The modulated PAM symbols are loaded on the imaginary component of the subcarriers at the first modulation depth of an ASE-DMT modulator while the real component are kept unused $X_1[k] = jB_1^{\mathrm{PAM}}[k]$, where $B_1^{\mathrm{PAM}}[k]$ is the PAM symbol at the k-th subcarrier of depth $d = 1$. At depth $d = 2$, the odd subcarriers are loaded with real valued PAM symbols $X_2[k] = A_2^{\mathrm{PAM}}[k]$, while all of the other subcarriers are kept unused. Therefore, the distortion caused by the clipping at zero level would only affect the real domain even subcarriers as shown in [7]. Subsequent streams can be generated at depth d, where the subcarriers will be loaded with real valued PAM symbols on the subcarriers $X_d[k'] = A_d^{\mathrm{PAM}}[k']$, where $k' = 2^{d-2}(2k+1)$ and $k = 0, 1, \cdots, N_{\mathrm{FFT}}/2^d - 1$. It was shown in [7] that the zero-level clipping is distortion-less to the information content at $X_d[2^{d-2}(2k+1)]$, and that all of the distortion will affect the subcarriers at $X_d[2^{d-1}k]$.

The distortion of the previous depths is estimated and canceled from the higher modulation depths in the successive clipping distortion cancellation process at the receiver. The modulated symbols of depth $d = 1$ is first obtained by considering the imaginary-valued components and by ignoring the real-valued components of the subcarriers. The demodulated symbols of depth $d = 1$ are then subtracted from the ASE-DMT received waveform. This would result in removing the imaginary component of the demodulated symbols and also removing the real domain distortion caused by the zero-level clipping of the depth $d = 1$ waveform. Subsequent depths can be demodulated by selecting the appropriate frequency subcarrier indexes at each depth. Further details on the modulation concept and the theoretical analysis of ASE-DMT can be found in [7].

The spectral efficiency at a modulation depth d is given as follows:

$$\eta_{\mathrm{ASE}}(d) = \frac{\log_2(M_{\mathrm{PAM}})N_{\mathrm{FFT},d}}{2^d(N_{\mathrm{FFT}} + N_{\mathrm{CP}})} \quad \text{bits/s/Hz}, \tag{1}$$

where $N_{\mathrm{FFT},d} = N_{\mathrm{FFT}} - 2$ for $d = 1$ and $N_{\mathrm{FFT},d} = N_{\mathrm{FFT}}$ for $d > 1$; M_{PAM} is the constellation size of PAM-DMT and ASE-DMT, N_{FFT} is the length of the OFDM frame and N_{CP} is the length of the cyclic prefix.

The performance of M_{PAM} in PAM-DMT and ASE-DMT is compared with the performance of M^2-QAM in DCO-OFDM. The spectral efficiency of ASE-DMT approaches twice the spectral efficiency of DCO-OFDM as the total number of depths increases. However, the energy efficiency comparison of both modulation techniques should be considered at an equivalent spectral efficiency. Therefore, the superimposed waveforms in ASE-DMT use smaller constellation sizes, $M_{\mathrm{PAM}} = \sqrt{M_{\mathrm{DCO}}}$, which can lead to an overall spectral efficiency that is equivalent to DCO-OFDM. The spectral efficiency of the first depth in ASE-DMT is equivalent to the spectral efficiency of a PAM-DMT modulation $\eta_{\mathrm{PAM}} = \eta_{\mathrm{ASE}}(1)$. The spectral efficiency of ASE-DMT can then be calculated as follows:

$$\eta_{\mathrm{ASE,T}}(D) = \sum_{d=1}^{D} \eta_{\mathrm{ASE}}(d) \quad \text{bits/s/Hz}. \tag{2}$$

The spectral efficiency of DCO-OFDM is given by (1) when substituting $d = 1$ and $M_{\mathrm{DCO}} = M_{\mathrm{PAM}}^2$. The performance of ASE-DMT is investigated in this paper for up to $D = 5$ modulation depths. The spectral efficiency of ASE-DMT increases as the total number of modulation depths D increases as shown in Fig. 1. For example, the spectral efficiency of ASE-DMT is 87.5% of the spectral efficiency of DCO-OFDM when $D = 3$. Therefore, an excess bandwidth is allocated for PAM-DMT and ASE-DMT techniques to allow the performance comparison with DCO-OFDM to be performed at the same data rate. The relative excess bandwidth as a function of the total number of modulation depths is shown in Fig. 1. ASE-DMT can additionally be realized by employing arbitrary constellation sizes to close any remaining spectral efficiency gap with a maximum of three modulation depths [7]. This solution is particularly useful for the cases where the excess bandwidth is not practically available due to the frequency profile constraints of the considered VLC system. However, the excess bandwidth required for $D > 3$ is marginal as shown in Fig. 1.

The modulated signals of DCO-OFDM, PAM-DMT and ASE-DMT are clipped to fit within the dynamic range of the used digital-to-analog converter (DAC) and the considered transmitter device. The clipping results in a limited distortion that is controlled by the upper and lower clipping points [10]. The DCO-OFDM modulation signal is clipped to both an upper and a lower clipping points given at $\pm 3.2\sigma_x$, where σ_x is the standard deviation of the modulation signal. These values were experimentally found to achieve the best BER performance after exhaustive experiments. The PAM-DMT and ASE-DMT modulation signals are both unipolar. Therefore, the lower clipping is set to zero and the upper clipping is set to $6.4\sigma_x$ to allow for a fair comparison at an equivalent quantization noise with DCO-OFDM. The OFDM frame length is set to $N_{\mathrm{FFT}} = 1024$ and the cyclic prefix length is set to $N_{\mathrm{CP}} = 5$ for all the considered modulation techniques. These values were also selected based on the BER performance after extensive experiments.

An estimation of the channel and the achievable signal-to-noise ratio (SNR) over the utilized bandwidth is obtained using a conventional mean estimator [9]. A zero-forcing equalizer is used to maintain a relatively constant SNR over all of the considered subcarriers.

III. Experimental Setup

The digital modulation signals are generated in MATLAB® and converted into analogue signals using the arbitrary waveform generator (AWG) (Agilent 81180A) with a $V_{\mathrm{PP}} = 2$ V for the blue LED and a $V_{\mathrm{PP}} = 125$ mV for the IR VCSEL. The current-voltage (I-V) and luminance-voltage (L-V) characteristic functions for both the blue LED and the IR VCSEL are shown in Fig. 2(a & b), respectively. The L-V characteristic function of the blue LED in Fig. 2(a) is shown to exhibit

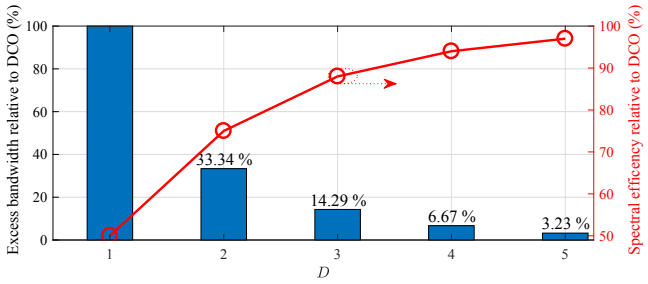

Fig. 1. The excess bandwidth required in ASE-DMT relative to DCO-OFDM as a function of the total number of modulation depths D.

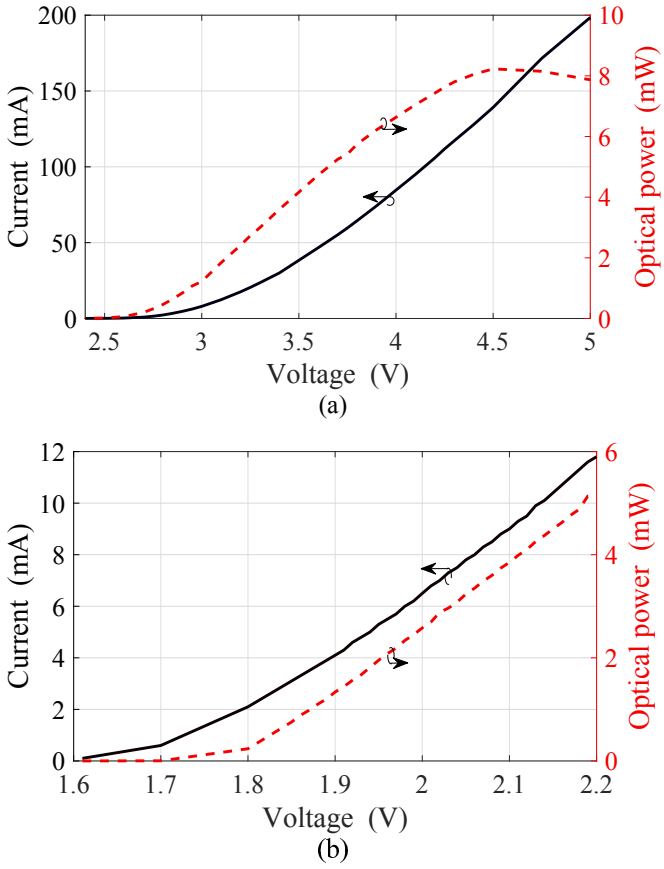

Fig. 2. (a) current-voltage and luminescence-voltage characteristics for: (a) the blue LED and (b) IR VCSEL.

higher nonlinearity in comparison with the L-V characteristic function of the IR VCSEL in Fig. 2(b). Therefore, the sensitivity of ASE-DMT to the nonlinearity of the optical source can be investigated by comparing the results of the blue LED and the IR VCSEL.

The ASE-DMT modulation signal is inherently unipolar. However, it is mapped to a bipolar signal at the DAC as the AWG is unable to generate unipolar outputs without a degradation of the resolution of the DAC . The AWG generates bipolar outputs with a DAC range between $-V_{\mathrm{PP}}/2$ and $V_{\mathrm{PP}}/2$. The DC bias is added to the modulation signals using a bias-tee (Mini-Circuits ZFBT-4R2GW+). The DC bias

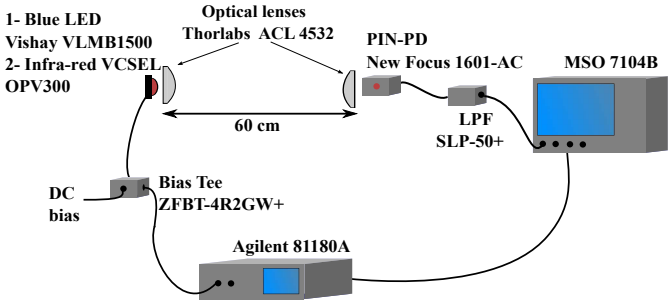

Fig. 3. The schematic setup of the experiment showing the optical system, AWG, oscilloscope, electrical filter and Bias-tee.

is required for the unipolar ASE-DMT signal due to the bipolarity of the AWG and the turn-on voltage of the used light source.

An optical system of two identical aspheric lenses (Thorlabs ACL 4532) is used at the photoreceiver and the transmitter ends as shown in Fig. 3. The communications link distance is 60 cm and the photoreceiver is a high speed positive-intrinsic-negative photodiodes (PIN-PD) (New Focus 1601-AC). An electrical low pass filter (SLP-50+) is used at the receiver with a pass-band between DC and 48 MHz to block any high RF interference. The received signal is captured at the oscilloscope (Agilent MSO7104B) and processed afterwards using MATLAB®.

IV. Results and Discussion

The performance of ASE-DMT is measured for a total number of depths $D = \{1, 3\}$ when using the IR VCSEL and for $1 \leq D \leq 5$ when using the blue LED. Note that D refers to the total number of modulation depths of the ASE-DMT waveform whereas d refers to the index of the superimposed stream at the modulation depth d, given that $1 \leq d \leq D$.

The BER and average SNR are measured for DCO-OFDM, PAM-DMT and ASE-DMT against the DC bias voltage V_{DC}, average electrical power $P_{\mathrm{elec}}^{\mathrm{avg}}$ and average optical power $P_{\mathrm{opt}}^{\mathrm{avg}}$. The voltage signal applied to the considered transmitter device by the AWG is captured by the oscilloscope during the transmission period. The corresponding I-V curve is used to estimate the corresponding current values. These allow for the average electrical power to be estimated for each of the used modulation signals using both the blue LED and the IR VCSEL. The average optical power is measured using the spectral irradiance head (Labsphere E1000) and the monochromatic optical power meter (Thorlabs S121C).

The BER performance for each of the superimposed streams of a 4-PAM ASE-DMT modulation with $D = 5$ is presented as a function of the average electrical power of the blue LED in Fig. 4. The average BER is calculated based on the relative spectral efficiency contribution of each of the modulation depths. The BER performance is shown to degrade as the modulation depth order d increases. However, the BER performance for all of the modulation depths converges to a similar BER value as the average electrical power increases. At high electrical average power, the error propagation becomes insignificant to affect the BER performance at the higher

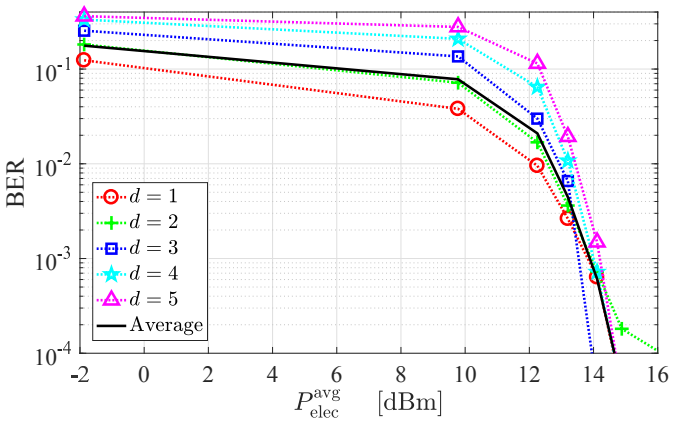

Fig. 4. The BER as a function of the average electrical power $P_{\text{elec}}^{\text{avg}}$ for each of the five superimposed modulation depths of a 4-PAM ASE-DMT waveform with $D = 5$. This is obtained for the blue LED.

modulation depth orders. This is due to the decrease in the number of wrongly decoded bits at the lower modulation depth orders. The average BER performance is shown to be heavily affected by the BER performance of the lower order modulation depths due to their higher spectral efficiency contribution. The number of transmitted PAM symbols at high modulation depth orders is small due to the selective loading algorithm as well as the limited memory size of the AWG. This reduces the statistical significance of the results at low BER values. In addition, this explains the small deviation of the BER values below 1×10^{-3}.

The average SNR values are measured against V_{DC} in Fig. 5 for DCO-OFDM, PAM-DMT and ASE-DMT. The average SNR of ASE-DMT is presented for $D = 3$. It is shown that PAM-DMT and ASE-DMT achieve higher SNR levels at low DC bias levels. The SNR gain in comparison with DCO-OFDM increases as the DC bias increases to reach a peak of 17.33 dB for PAM-DMT and 14.27 dB for ASE-DMT at $V_{\text{DC}} = 1.8$ V. The SNR gain of PAM-DMT is higher in comparison with ASE-DMT. However, this comes at the price of using 85.71% extra excess bandwidth as shown in Fig. 1. The SNR gain of ASE-DMT drops due to the clipping distortion and diminishes at 1.9 V. The SNR degradation at high DC bias values of PAM-DMT and ASE-DMT is in agreement with the SNR degradation of DCO-OFDM due to clipping distortion. However, the SNR degradation of PAM-DMT and ASE-DMT is shown to be higher due to their unipolar distributions. In comparison with DCO-OFDM, a larger number of signal samples in PAM-DMT and ASE-DMT are subject to distortion by the upper saturation point of the IR VCSEL.

The minimum required optical power levels to achieve a BER at the forward error correction (FEC) threshold (3.8×10^{-3}) are presented in Fig. 6(a & b) as a function of the spectral efficiency when using the blue LED and the IR VCSEL, respectively. The results of ASE-DMT are presented for $1 \leq D \leq 5$ when using the blue LED and for $D = 1$ and $D = 3$ when using the IR VCSEL. The results for the IR VCSEL are presented for two representative cases to allow for a comparison with the trends obtained using the blue LED.

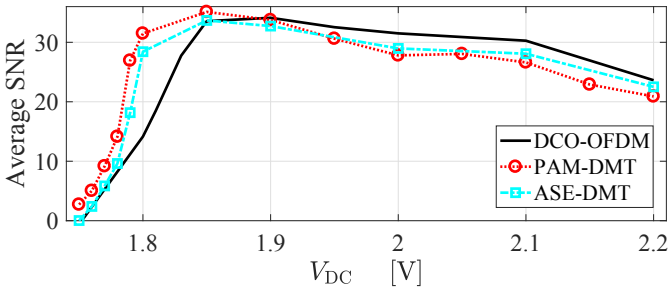

Fig. 5. The average SNR versus bias voltage V_{DC} for DCO-OFDM, PAM-DMT and ASE-DMT when $D = 3$.

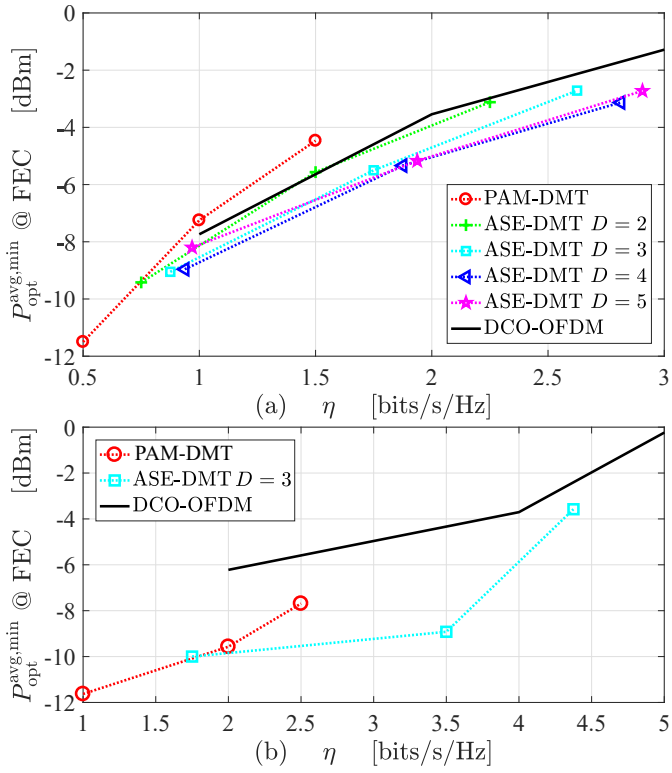

Fig. 6. The minimum average optical power $P_{\text{opt}}^{\text{avg,min}}$ required at a BER equals to the FEC threshold 3.8×10^{-3} versus the spectral efficiency of DCO-OFDM and ASE-DMT with a total number of depths $D = 1$ and $D = 3$ using (a) the blue LED and (b) the IR VCSEL.

The comparison in Fig. 5 is performed at the same data rate. Therefore, a considerable excess bandwidth equal to the whole utilized bandwidth in DCO-OFDM is required for PAM-DMT. The results in Fig. 6(a & b) are presented at a normalized bandwidth to allow for a fair comparison between PAM-DMT and the different values of D in ASE-DMT.

The required optical average power $P_{\text{opt}}^{\text{avg,min}}$ is shown in Fig. 6(a) for the blue LED. The improvement in the optical average power of ASE-DMT with $D = 4$ at $\eta = 1$ bits/s/Hz approaches 1 dB when compared with DCO-OFDM. However, the optical power savings increases as the spectral efficiency increases. The reduction in the required optical power reaches 1.5 dB at $\eta = 2$ bits/s/Hz and 1.45 dB at $\eta = 2.5$ bits/s/Hz when $D = 4$. The improvements in the optical power

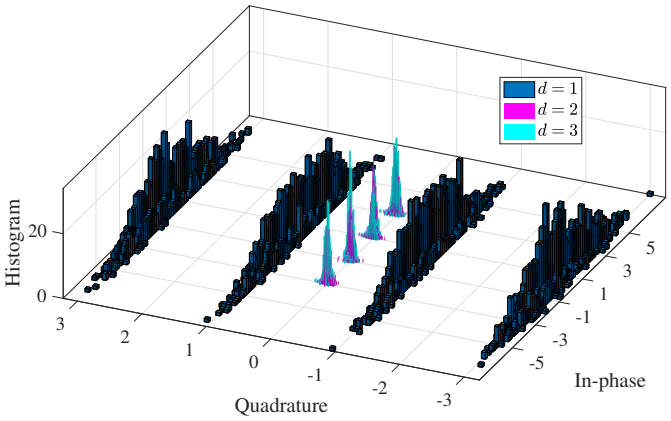

Fig. 7. The histogram of the demodulated symbols constellations of 4-PAM ASE-DMT with a total number of depths $D = 3$. The constellations are shown for the superimposed modulation depths $d = \{1, 2, 3\}$. The demodulated symbols are obtained when using the IR VCSEL with a bias voltage $V_{\mathrm{DC}} = 1.85$V.

requirements are higher for the case of the IR VCSEL as shown in Fig. 6(b). The optical power gain is estimated at 3.63 dB for ASE-DMT when $D = 3$. This is mainly due to the improved linearity of the L-V characteristic of the IR VCSEL. The differences in the optical power requirements for the same modulation technique between the blue LED and the IR VCSEL are also attributed to the higher responsivity of the photoreceiver at the IR band. This allows the optical power levels of the IR VCSEL shown in Fig. 6(b) to be lower than the optical power levels of the blue LED shown in Fig. 6(a). ASE-DMT needs less optical power than DCO-OFDM to operate at the same data rate and the same BER. Therefore, ASE-DMT can support longer distance VLC links with more relaxed alignment/orientation constraints at the receiver.

The demodulated constellation diagram for 4-PAM ASE-DMT is presented in Fig. 7. The constellation points for each of the modulation depths are obtained using the iterative demodulation process as explained in Section II. The constellation diagram is obtained at a bias voltage $V_{\mathrm{DC}} = 1.85$ V for the IR VCSEL. The demodulated symbols are shown in the constellation diagrams with a total number of modulation depths $D = 3$. The constellation points are given for the superimposed modulation depths $d = \{1, 2, 3\}$. The histogram shows the distribution of the constellation points against the number of demodulated symbols. The information bits are conveyed in the imaginary component of the symbols at the first modulation depth when $d = 1$. The rest of the superimposed modulation depths are conveyed in the real component of the symbols. The bias levels represent the optimal bias point for ASE-DMT with the used transmitter devices. This explains the good representation of the constellation points which allows for ASE-DMT performance to reach the BER floor.

V. Conclusions

The proposed ASE-DMT is demonstrated as a promising choice for energy efficient LiFi systems. The SNR performance gain of ASE-DMT at low DC bias results in reduced electrical and optical power requirements in comparison with DCO-OFDM and PAM-DMT. ASE-DMT is a promising choice for any IM/DD system where a reduction of energy consumption is required. An example of a potential application is the IR-based uplink of a LiFi system where ASE-DMT is shown to be a favorable solution for long distance IM/DD systems. ASE-DMT is also a better choice than DCO-OFDM at low DC bias where dimming of the light source is required.

The degradation of ASE-DMT at high optical power restricts the capability of the system to satisfy high illumination requirements. In addition, the inability to drive the transmitter device at a high DC bias results in a reduced 3-dB bandwidth of the considered transmitter. Therefore, it can be concluded that ASE-DMT is a less favorable choice when compared with DCO-OFDM at high DC bias points where the energy efficiency of the system is not the main concern. A possible solution for using ASE-DMT at high DC bias levels could be the inversion of the polarity of the ASE-DMT waveform. The details of this investigation will be the subject of our future research.

Acknowledgment

The authors acknowledge support by the UK Engineering and Physical Sciences Research Council (EPSRC) under Grants EP/R007101/1 and EP/M506515/1. Prof. H. Haas also acknowledges the financial support of his research by the Wolfson Foundation and the Royal Society.

References

[1] Cisco Visual Networking Index, "The Zettabyte Era: Trends and Analysis," Retrieved from https://www.cisco.com/c/en/us/solutions/collateral/service-provider/visual-networking-index-vni/vni-hyperconnectivity-wp.html, Jun. 2017.

[2] D. Tsonev, S. Videv, and H. Haas, "Towards a 100 Gb/s Visible Light Wireless Access Network," *OSA Opt. Express*, vol. 23, no. 2, pp. 1627–1637, Jan 2015. [Online]. Available: http://www.opticsexpress.org/abstract.cfm?URI=oe-23-2-1627

[3] S. Dimitrov and H. Haas, *Principles of LED Light Communications: Towards Networked Li-Fi*. Cambridge University Press, 2015.

[4] H. Haas, L. Yin, Y. Wang, and C. Chen, "What is LiFi?" *IEEE/OSA J. Lightw. Technol.*, vol. 34, no. 6, pp. 1533–1544, Mar. 2016.

[5] M. Islim, D. Tsonev, and H. Haas, "A Generalized Solution to the Spectral Efficiency Loss in Unipolar Optical OFDM-based Systems," in *Proc. of the International Conference on Communications (ICC)*. London, UK: IEEE, Jun., 8–12 2015.

[6] S. C. J. Lee, S. Randel, F. Breyer, and A. M. J. Koonen, "PAM-DMT for Intensity-Modulated and Direct-Detection Optical Communication Systems," *IEEE Photon. Technol. Lett.*, vol. 21, no. 23, pp. 1749–1751, Dec. 2009.

[7] M. S. Islim and H. Haas, "Augmenting the Spectral Efficiency of Enhanced PAM-DMT-based Optical Wireless Communications," *OSA Opt. Express*, vol. 24, no. 11, pp. 11 932–11 949, May 2016. [Online]. Available: http://www.opticsexpress.org/abstract.cfm?URI=oe-24-11-11932

[8] Q. Wang, B. Song, B. Corcoran, L. Zhuang, and A. J. Lowery, "Real-Time Demonstration of Augmented-Spectral-Efficiency DMT Transmitter Using a Single IFFT," *IEEE/OSA J. Lightwave Technol.*, vol. 35, no. 21, pp. 4796–4803, Nov 2017.

[9] D. Tsonev, S. Videv, and H. Haas, "Unlocking Spectral Efficiency in Intensity Modulation and Direct Detection Systems," *IEEE J. Sel. Areas Commun.*, vol. 33, no. 99, pp. 1758–1770, 2015.

[10] S. Dimitrov, S. Sinanovic, and H. Haas, "Clipping Noise in OFDM-Based Optical Wireless Communication Systems," *IEEE Trans. on Commun.*, vol. 60, no. 4, pp. 1072–1081, April 2012.